Intra *c*-axis dimer hybridization and mixed valency in Mg-doped Ti_2O_3

T. Miyoshino,[1] D. Takegami,[2] A. Meléndez-Sans,[2] R. Nakamura,[1] M. Yoshimura,[3] K.-D. Tsuei,[3] K. Takasu,[4] T. Okuda,[4] L. H. Tjeng,[2] and T. Mizokawa[1]

[1]*Department of Applied Physics, Waseda University, Shinjuku, Tokyo 169-8555, Japan*
[2]*Max Planck Institute for Chemical Physics of Solids, 01187 Dresden, Germany*
[3]*National Synchrotron Radiation Research Center, 30076 Hsinchu, Taiwan*
[4]*Graduate School of Science and Engineering, Kagoshima University, Kagoshima 890-0065, Japan*

(Received 21 December 2022; accepted 7 March 2023; published 23 March 2023)

We have studied the Ti^{3+}/Ti^{4+} mixed valence state in Mg-doped Ti_2O_3 using hard x-ray photoemission spectroscopy. The Ti $2p$ spectrum for the corundum-type Ti_2O_3 revealed the Ti^{3+} configuration with strong electronic coupling in the *c*-axis Ti-Ti pairs whereas the data for the ilmenite-type $MgTiO_3$ confirmed the Mg^{2+}-Ti^{4+} charge state in the *c*-axis cation pairs. In $Mg_{0.29}Ti_{1.71}O_3$, the Ti $2p$ spectrum hardly showed the Ti^{4+} peak, which was in $MgTiO_3$ indicating that the *c*-axis pairing of the Mg is with a Ti^{3+} ion rather than a Ti^{4+} and that the Ti^{3+}/Ti^{4+} mixed valence state is materialized within the Ti-Ti *c*-axis pairs. In $Mg_{0.63}Ti_{1.37}O_3$, we detected the presence of Mg^{2+}-Ti^{4+} pairs. The results indicate the important role of hybridization within the *c*-axis pairs not only in the Ti^{3+}-Ti^{3+} configuration, but also above all in the Ti^{3+}/Ti^{4+} mixed valence state, superseding the Madelung energy gain of the Mg^{2+}-Ti^{4+} *c*-axis pair formation.

DOI: 10.1103/PhysRevB.107.115145

I. INTRODUCTION

Several transition-metal oxides exhibit dimerization or trimerization of the transition-metal ions in which the *d*-orbital degrees of freedom play an essential role to form a stable molecular orbital state within the dimers or trimers [1–3]. For example, the Ti-Ti dimers are formed due to the orbitally assisted Peierls mechanism in the spinel-type $MgTi_2O_4$ providing its unique metal-insulator transition [4–6]. In the spinel structure, the Ti pyrochlore lattice is constructed from the edge-sharing TiO_6 octahedra. Without the distortion, Ti-Ti pairs are not explicitly seen in the pyrochlore lattice. Another striking example of the Ti-Ti molecular orbital formation is known in corundum-type Ti_2O_3 [7–10]. In contrast to the spinel structure, Ti-Ti pairs of face-sharing TiO_6 octahedra already exist in the corundum structure as shown in the left panel of Fig. 1. The Ti-Ti distance of the pair is gradually shortened in going from 600 to 400 K, and Ti_2O_3 undergoes a metal-to-insulator transition [7–10]. The reduction of the Ti-Ti distance can be viewed as a dimerization or the formation of Ti^{3+}-Ti^{3+} molecules. From the theoretical viewpoints, the Ti $3d$ a_{1g} states play the vital role for forming the molecular orbitals and stabilizing the insulating state [11–15]. The molecular orbitals of the a_{1g} states are experimentally confirmed by x-ray absorption spectroscopy [16] and photoemission spectroscopy [17].

It is interesting to study effect of doping in these materials with Ti-Ti dimers. Indeed, Mg substitution for Ti in the spinel-type $Mg_{1+x}Ti_{2-x}O_4$ system induces localized Ti spins and generates intriguing magnetic properties [18], suggesting that the Ti-Ti dimers are quickly disturbed. A recent x-ray absorption and photoemission study [19] revealed that the $3d$ electrons are relatively localized at each Ti site, making it plausible that the formation energy of the dimers is relatively small. The situation for Ti_2O_3 could be rather different. There, the Ti-Ti pairs or dimers along the *c* axis in the face-sharing octahedra are structurally always present at all temperatures. The interesting question now is how the extra charge will be distributed over that lattice with Mg substitution for Ti in the $Mg_yTi_{2-y}O_3$ system. One can envision two possibilities. The first is that the Ti^{3+}-Ti^{3+} dimers survive with the Mg^{2+} ion being paired along the *c* axis with an isolated Ti^{4+} ion. The second is that the Ti-Ti dimers consist of Ti^{3+}-Ti^{4+} with the Mg^{2+} ion paired with an isolated Ti^{3+} ion. Since the Ti-Ti distance along the *c* axis is shorter than those on the *ab* plane in Ti_2O_3, the first possibility would take the advantage of having the excitonic Madelung energy of Mg^{2+}-Ti^{4+} inside the face-sharing octahedra instead of the Mg^{2+} and Ti^{4+} sites being further apart.

We note that ilmenite-type $MgTiO_3$ (right panel of Fig. 1), the $y = 1$ end member of $Mg_yTi_{2-y}O_3$ is by itself a well-studied titanate, which is a band insulator with an energy gap of ∼3.05 eV. It has been attracting great interest due to its photochemical activities [20,21] similar to TiO_2 with edge-sharing TiO_6 octahedra. When Ti $3d$ electrons are introduced in $MgTiO_3$ by Ti substitution for Mg, the mixed valence of Ti^{3+} and Ti^{4+} in the face-sharing octahedra may resemble those of $Ti_{1-x}Nb_xO_2$ [22] and hollandite-type $Ba_xTi_8O_{16}$ [23,24] in the edge-sharing octahedra. However, the Ti^{3+} and Ti^{4+} mixed valence state in the face-sharing octahedra is not well studied by means of photoemission spectroscopy compared to that in the edge-sharing ones. Ti-Ti dimers are hardly created in the edge-sharing systems, which is consistent with the quick destruction of the Ti-Ti dimers in $Mg_{1+x}Ti_{2-x}O_4$. In $Mg_yTi_{2-y}O_3$ with the face-sharing octahedra, the Ti-Ti molecules would be formed at a certain level of *y* if they are robust against the Mg substitution for Ti.

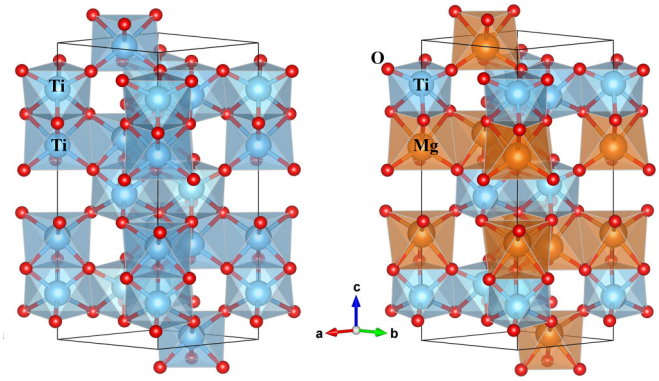

FIG. 1. Drawings for the crystal structure of Ti_2O_3 (left) and $MgTiO_3$ (right) created by VESTA [25].

In this context, it is very interesting to carry out a systematic study on the impact of Mg substitution for Ti in Ti_2O_3 or Ti substitution for Mg in $MgTiO_3$. In the present paper, we report hard x-ray photoemission spectroscopy (HAXPES) of $Mg_yTi_{2-y}O_3$ ($y = 1 - x$) with $y = 0.01$, 0.29, 0.63, and 1.00 in order to study the interplay between the Ti^{3+}-Ti^{3+} molecular orbital formation and the Ti^{3+}/Ti^{4+} mixed valence.

II. EXPERIMENT

Single-crystal samples of $Mg_yTi_{2-y}O_3$ with $y = 0.01, 0.29, 0.63$, and 1.00 (nominal Ti valence of $Ti^{+3.005}$, $Ti^{+3.17}$, $Ti^{+3.46}$, and $Ti^{+4.00}$, respectively) were grown as reported in the literature [26]. HAXPES measurements were performed at the Max-Planck-NSRRC HAXPES end station with a MB Scientific A-1 HE analyzer at the Taiwan undulator beamline BL12XU of SPring-8 [27]. The photon energy was set to 6.5 keV that has a probing depth of about 10 nm. The x-ray incidence angle was about 15° with respect to the sample surface, and the photoelectron detection angle was 90° with respect to the incident x rays. The diameter of the beam spot was about 50 μm. The crystals were fractured under ultrahigh vacuum of 10^{-6} Pa at 300 K in order to obtain atomically clean surfaces. The measurements were performed at 300 K. The total energy resolution was about 300 meV. The binding energy of the HAXPES spectra was calibrated using the Fermi edge of Au.

III. RESULTS AND DISCUSSION

Figure 2(a) shows survey scans for $Mg_yTi_{2-y}O_3$ with $y = 0.01$, 0.29, 0.63, and 1.00. The Mg 1s, Ti 2s/2p, and O 1s peak intensities are generally consistent with the compositions taking into account the photoionization cross sections [28–31]. Figure 2(b) displays a closeup of the C 1s region. There is no discernible C 1s signal visible indicating the cleanliness of the fractured surfaces. Figures 2(c) and 2(d) show a closeup of the Mg 2s peak and fine scans for the Mg 1s peak. The spectra are normalized to make the intensity of the Ti $2p_{3/2}$ component (estimated by the Gaussian fitting, which will be discussed later) proportional to the Ti content. The Mg 1s peak intensities of $y = 0.29$ and $y = 0.63$ samples are about 30% and 50% of that of $y = 1.00$, roughly consistent

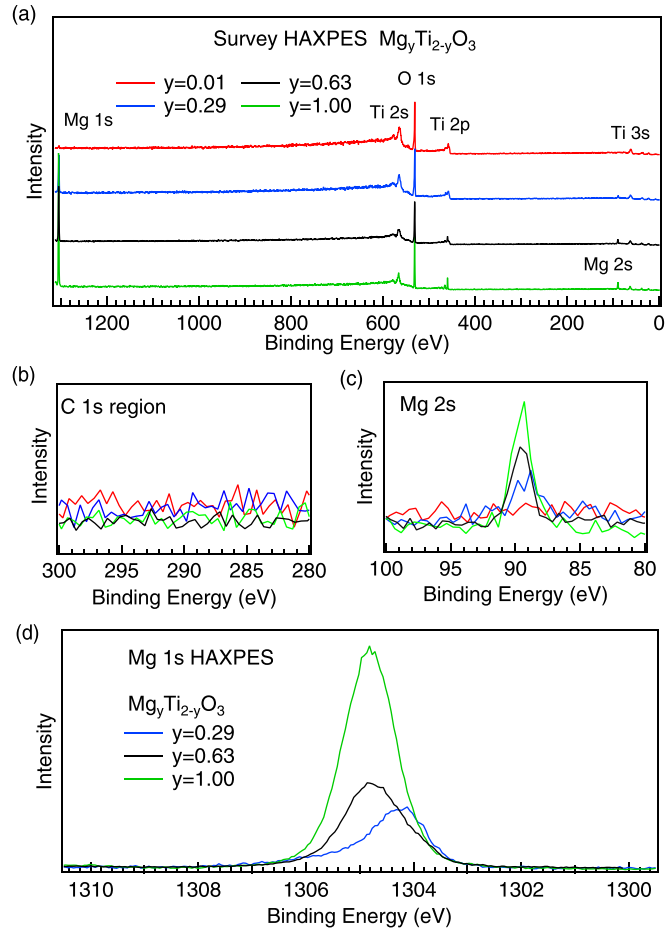

FIG. 2. (a) Survey scans, (b) C 1s, (c) Mg 2s, and (d) Mg 1s HAXPES of $Mg_yTi_{2-y}O_3$ with $y = 0.01$, 0.29, 0.63, and 1.00.

with the Mg content. The Mg 1s binding energy of $y = 0.29$ is by ~1 eV lower than those of $y = 0.63$ and 1.00. This is probably due to the Mg substitution in the relatively compact TiO_6 octahedron of Ti_2O_3. The average Ti-O distance is about 2.05 Å in Ti_2O_3 whereas the average Mg-O distance is about 2.12 Å in $MgTiO_3$. Therefore, the Mg-O distance tends to be shortened in $y = 0.29$ causing an increase in the magnitude of the Madelung potential at the Mg site (decrease in the Mg 1s binding energy). The tail on the higher binding energy side of $y = 0.29$ suggests minor Mg sites with longer Mg-O distance. A similar binding energy shift of ~1 eV is observed in $Ba_3Nb_5O_{15}$ where the compact Ba site with a shorter Ba-O distance exhibits lower binding energy than the spacious Ba site with a longer Ba-O distance [32].

Figure 3 shows the O 1s peaks. Although the O 1s peak of $y = 1.00$ is sharp and almost symmetric, it is broad and accompanied by tails on the higher binding energy side for $y = 0.01$, 0.29, and 0.63. This suggests the presence of different chemical environments for oxygens due to the Ti substitution for Mg on the ilumenite $MgTiO_3$. The O 1s spectra are fitted to two Gaussian functions as shown by the dotted curves in Fig. 3. Gaussian components are indicated by the dashed curves. In the bottom panel of Fig. 3, the O 1s peak energy is plotted as a function of y in $Mg_yTi_{2-y}O_3$. In going from $y = 0.01$ to $y = 0.29$, the O 1s peak energy decreases by

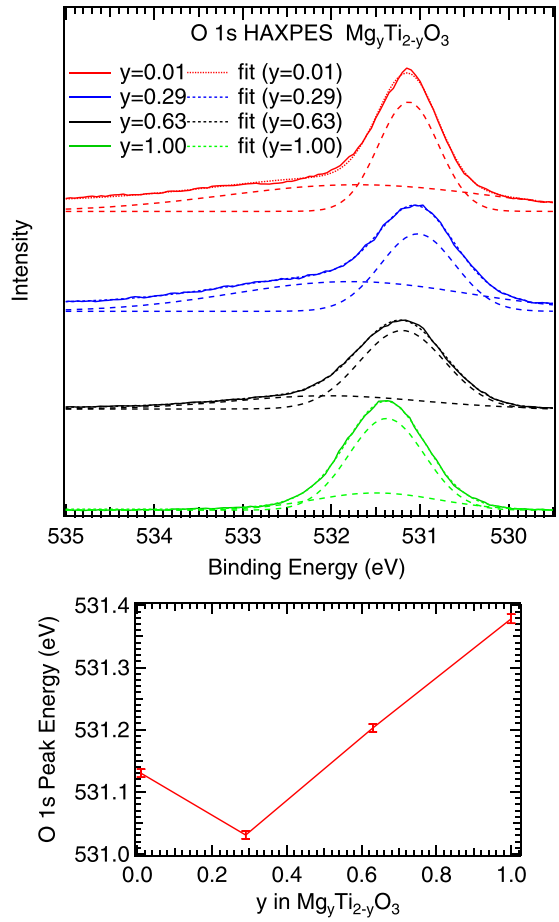

FIG. 3. O 1s HAXPES of $Mg_yTi_{2-y}O_3$ with $y = 0.01$, 0.29, 0.63, and 1.00. The dotted curves indicate the fitted results for the O 1s spectra. Shirley-type background is included in the fitted results. Gaussian components are represented by the dashed curves. In the bottom panel, the O 1s peak energy is plotted as a function of y. The vertical error bars indicate the uncertainties of the peak positions, estimated from the uncertainty of the fits and the uncertainty of the photon energy.

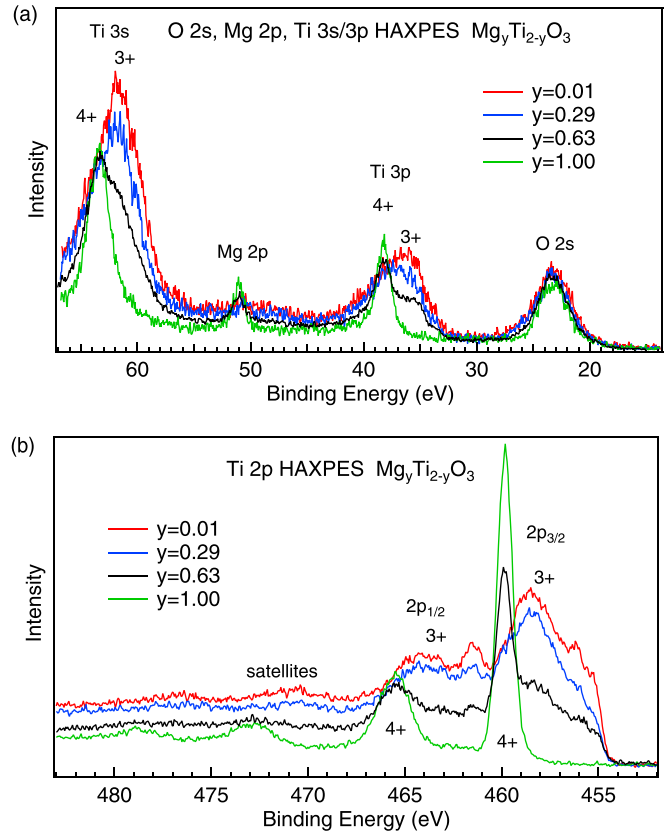

FIG. 4. (a) O 2s, Mg 2p, and Ti 3s/3p HAXPES spectra and (b) Ti 2p HAXPES spectra of $Mg_yTi_{2-y}O_3$ with $y = 0.01$, 0.29, 0.63, and 1.00.

0.1 eV. If Ti_2O_3 is viewed as a Mott insulator accompanied with the Ti-Ti molecules, the energy shift can be assigned to the downwards chemical potential shift by hole doping to the Mott insulating state. The O-1s peak energy increases from $y = 0.29$ to $y = 0.63$ indicating that the picture of hole-doped Mott state is not applicable for $y > 0.29$. On the other hand, the evolution from $y = 1.00$ to 0.63 corresponds to electron doping to $MgTiO_3$ which is a band insulator. The O 1s binding energy gradually decreases in going from $y = 1.00$ to 0.63 to 0.29 probably due to the band-gap reduction of $MgTiO_3$ by the Ti substitution for Mg.

Figure 4(a) shows the Ti 3s and Ti 3p peaks as well as the O 2s and Mg 2p peaks. The behavior of the Mg 2p peak is consistent with that of the Mg 1s peak. At $MgTiO_3$, the Ti 3s/3p peaks are sharp and have higher binding energy, consistent with the pure Ti^{4+} state. In going from $y = 0.63$ to 0.29 to 0.01, the Ti 3s and Ti 3p spectral distributions are broadened and shifted to the lower binding energy side. Figure 4(b) shows the Ti 2p spectra for $Mg_yTi_{2-y}O_3$ with $y = 0.01$, 0.29, 0.63, and 1.00. $MgTiO_3$ exhibits the sharp Ti $2p_{3/2}$ and Ti $2p_{1/2}$ peaks (around 460 and 466 eV), which are accompanied by the charge transfer satellites (around 473 and 479 eV). This is consistent with Ti 3s and Ti 3p peaks indicating the pure Ti^{4+} state in the ilumenite-type $MgTiO_3$. The $y = 0.63$ sample exhibits Ti^{4+} and Ti^{3+} components indicating the mixed valence state. The Ti 2p spectrum of $y = 0.01$ is very similar to that of Ti_2O_3 [17,33,34]. The spectral shape of $y = 0.01$ including the satellite peaks on the lower binding energy at about 455 and 456 eV can be reproduced by the Ti_2O_9 cluster model calculation [17]. In this cluster model, the two TiO_6 octahedra share the face, and the Ti-Ti distance is relatively small. The Ti-3d a_{1g} orbitals of the two Ti sites are strongly hybridized with each other and provide the bonding-antibonding energy splitting in the Ti-Ti molecule. The screening channels due to the a_{1g}-a_{1g} hybridization are responsible for the satellite peaks on the lower binding energy. In going from $y = 0.01$ to $y = 0.29$, the area sum of the satellite peaks at about 455 and 456 eV is considerably reduced. This indicates that the screening effect in the Ti^{3+}-Ti^{3+} pairs is reduced in $y = 0.29$. If the remaining Ti^{3+}-Ti^{3+} pairs are the same as those of Ti_2O_3, the isolated Ti site paired with Mg^{2+} is expected to be +4. However, in the Ti 2p spectrum of $y = 0.29$, we observe that there are no clear Ti^{4+} peaks, such as in $y = 0.63$, and instead, only faint shoulders are observed at about 460 eV. This suggests that the isolated Ti site is mostly +3, and electrons are mainly

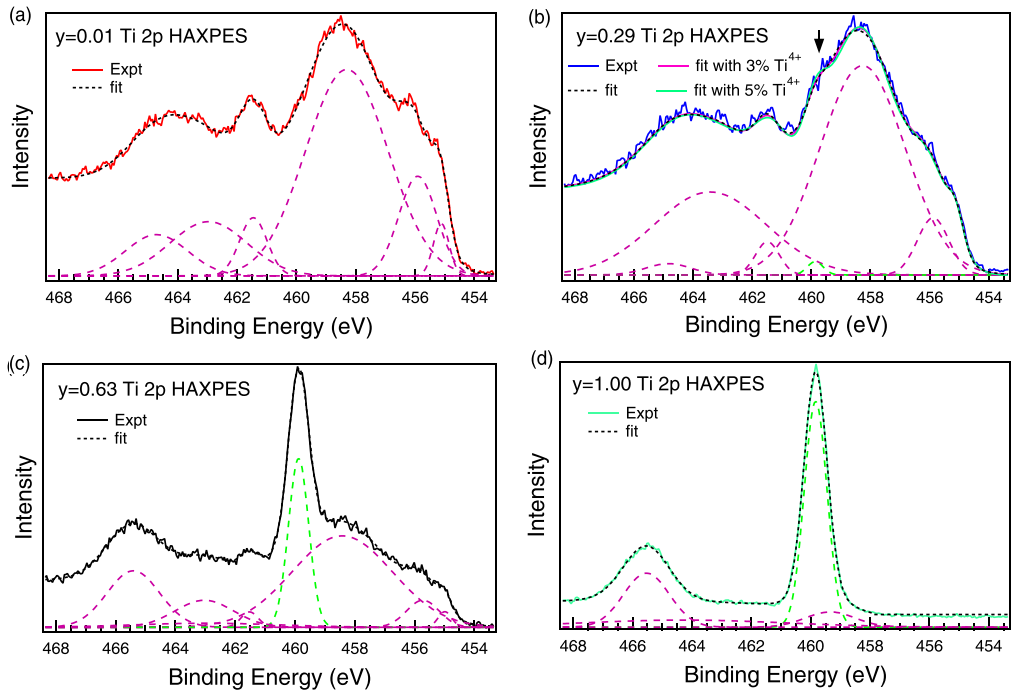

FIG. 5. Curve fits for the Ti $2p$ HAXPES spectra of $Mg_yTi_{2-y}O_3$ with (a) $y = 0.01$, (b) $y = 0.29$, (c) $y = 0.63$, and (d) $y = 1.00$. The dashed curves indicate each Gaussian functions. For $y = 0.29$, curve fits with 3% Ti^{4+} and 5% Ti^{4+} are shown by the solid curves. The Ti^{4+} component is indicated by the arrow. The Shirley-type background is included in the fitted results.

removed from the Ti^{3+}-Ti^{3+} pairs resulting in the hole-doped Ti-Ti pairs or the Ti^{3+}/Ti^{4+} mixed valence Ti-Ti pairs.

Figure 5 shows fitting results of the Ti $2p$ spectra. The complicated Ti^{3+} components are fitted to six Gaussian functions (including $2p_{3/2}$ and $2p_{1/2}$ branches) for $y = 0.01$. On the other hand, the Ti^{4+} components are fitted to two Gaussian functions for the $2p_{3/2}$ and $2p_{1/2}$ peaks of $y = 1.00$. The Ti $2p_{3/2}$ branch of $y = 0.01$ is expressed by the three Gaussians. The two Gaussians at the lower binding energy side represent the screening effect in the Ti-Ti pairs. When one of the Ti ions in the Ti-Ti pairs is replaced by Mg, the other Ti ion becomes isolated and expected to be Ti^{4+}. Indeed, the Ti $2p$ spectrum of $y = 0.63$ exhibits such Ti^{4+} peaks and, therefore, is fitted to eight Gaussian functions. In the Ti $2p_{3/2}$ branch, the ratio of the isolated Ti^{4+} peak area to the total area is estimated to be 0.25 from the fitting. At $y = 0.63$, 31.5% of the cation sites are occupied by Mg. Here, one can assume that 17% of the cation sites are occupied by Ti^{4+} which are paired with Mg^{2+} in the face-sharing octahedra. Then, 14.5% of the cation sites are occupied by Ti^{3+} paired with Mg^{2+}. The remaining 37% cation sites can be assigned to the hole-doped Ti-Ti pairs. Since the hole concentration per formula unit is 0.63, the hole-doped Ti-Ti pairs are expected to accommodate $0.63–1.37\times0.25 = 0.29$ holes per formula unit. The rough estimation suggests that each hole-doped pair accommodates $0.29/0.37 \sim 0.8$ holes.

Although isolated Ti^{4+} sites are expected also at $y = 0.29$, Ti^{4+} peaks are not clearly seen in the Ti $2p$ spectrum of $y = 0.29$. When we tried to fit the Ti $2p$ spectrum to eight Gaussians in the similar manner for $y = 0.63$, no convergence was obtained. Instead, we fixed the peak positions of Ti^{4+} components to those of $y = 0.63$ and forcibly fitted the spectrum to eight Gaussians. In the fitted result shown by the dashed curve in Fig. 5(b), the Ti^{4+} component is about 1% of Ti^{3+}. In addition, we tried to fit the spectrum assuming 3% Ti^{4+} and 5% Ti^{4+}. The obtained curve fits shown by the solid curves are acceptable, but the residual sum of squares increases with increasing the Ti^{4+} component due to narrowing of the main Ti^{3+} peak. From the different fitting procedures, we can estimate the best fit value and the upper limit value of Ti^{4+} amount to be about 1% of Ti^{3+} and 5% of Ti^{3+}, respectively, which are far below 20.5% (0.17/0.83, the value expected from the scenario where the isolated ions are Ti^{4+}). Here, we neglect the isolated Ti^{4+} weight and estimate hole concentration in the Ti-Ti pair. At $y = 0.29$, 14.5% of the cation sites are occupied by Mg. Since there is no isolated Ti^{4+}, 14.5% of the cation sites are occupied by Ti^{3+} paired with Mg^{2+}, and 71% of the cation sites can be assigned to the hole-doped Ti-Ti pairs. Since the hole concentration per formula unit is 0.29, each hole-doped Ti-Ti pair is expected to accommodate $0.29/0.71 \sim 0.4$ holes. The area sum of the low binding energy components at about 455 and 456 eV relative to the area of the high binding energy Ti^{3+} component at 458.5 eV is 0.2698, 0.1311, and 0.1287 for the $y = 0.01$, 0.29, and 0.63 samples, respectively. This indicates that, apart from the isolated Ti^{4+} and Ti^{3+} sites, the remaining Ti-Ti pairs are still affected by the Ti-Ti charge transfer in the face-sharing octahedra even in $y = 0.63$, although the average Ti-Ti distance gets much longer than that in Ti_2O_3 [26].

Figure 6 shows the valence-band spectra. The Ti $3d$ band evolves near the Fermi level in going from $y = 0.00$ to $y = 0.01$. At $y = 0.01$, the Ti $3d$ peak is located around 0.5 eV

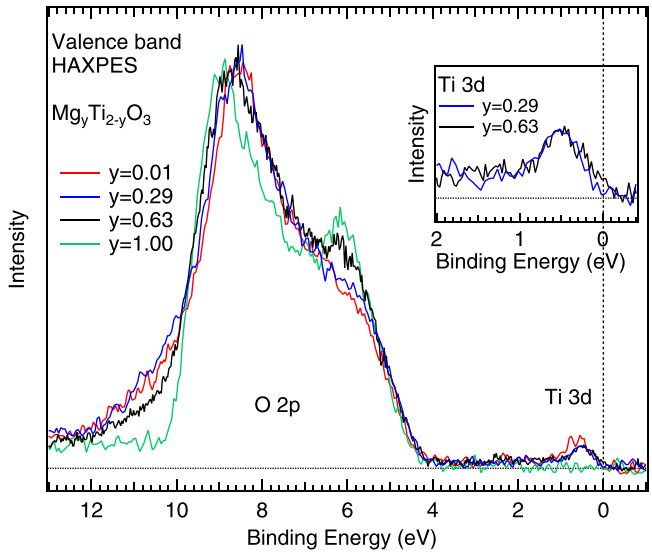

FIG. 6. Valence-band HAXPES of $Mg_yTi_{2-y}O_3$ with $y = 0.01$, 0.29, 0.63, and 1.00. The spectra are roughly normalized by the peak height of the O $2p$ band. The inset shows the Ti $3d$ band near the Fermi level for $y = 0.29$ and 0.63.

below the Fermi level which is consistent with the HAXPES report on Ti_2O_3 [17]. The Ti $3d$ peak position does not depend on the doping level y. At $y = 0.29$, the Ti $3d$ spectral weight at the Fermi level is still very small as shown in the inset. This is consistent with the surviving Ti-Ti molecules suggested by the Ti $2p$ spectra. Although the isolated Ti site is +3 with the localized Ti $3d$ electron, the a_{1g}-a_{1g} bonding orbitals in the Ti-Ti dimers are partially occupied causing additional disorders, which may suppress lattice thermal conductivity just like the brookite system [35]. On the other hand, at $y = 0.63$, appreciable Ti $3d$ spectral weight is observed at the Fermi level. This is probably consistent with the deviation from the hole-doped Mott state seen in the O $1s$ peak energy shift. Since the c axis or the direction of the a_{1g} orbital is roughly perpendicular to the photoemission direction in the present measurements, the photoionization cross section of Ti $3d$ tends to be reduced in $y = 0.01$ and 0.29 due to the proportionality of the transition matrix element effect to the initial-state orbitals in this particular experimental geometry [36]. On the other hand, the photoionization cross section of Ti $3d$ is less reduced in $y = 0.63$ since the e_g^π orbitals tend to be occupied due to the increased Ti-Ti distance in the face-sharing TiO_6 octahedra, resulting in the observed similar spectral weights of the Ti $3d$ feature despite with increasing y.

IV. CONCLUSION

We have performed HAXPES measurements on $Mg_yTi_{2-y}O_3$ with $y = 0.01$, 0.29, 0.63, and 1.00. The Ti $2p$ spectrum for $y = 0.01$ resembles that of Ti_2O_3 indicating Ti^{3+} configuration with strong Ti-Ti electronic coupling in the c-axis cation pair of the face-sharing octahedra. On the other hand, the Ti $2p$ spectrum for $y = 1.00$ shows the Mg^{2+}-Ti^{4+} charge state in the pair. In $y = 0.29$, the Ti $2p$ spectrum hardly shows the Ti^{4+} peak, which was in $y = 1.00$, indicating the c-axis pairing of Mg^{2+} and Ti^{3+} and the Ti^{3+}/Ti^{4+} mixed valence state in the Ti-Ti c-axis pairs. In $y = 0.63$, the Ti $2p$ spectrum exhibits the Ti^{4+} signature similar to $y = 1.00$ indicating existence of the Mg^{2+}-Ti^{4+} pairs. The results indicate the important role of hybridization within the c-axis cation pairs not only in the Ti^{3+}-Ti^{3+} configuration, but also in the Ti^{3+}/Ti^{4+} mixed valence state. The electronic energy gain in the mixed valence Ti-Ti pairs prevails the Madelung energy gain of the Mg^{2+}-Ti^{4+} c-axis pair formation.

ACKNOWLEDGMENT

We acknowledge the overall support from SPring-8. This work was supported by a Grant-in-Aid from the Japan Society of the Promotion for Science (JSPS) (Grant No. JP22H01172).

[1] D. I. Khomskii, *Transition Metal Compounds* (Cambridge University Press, Cambridge, UK, 2014).
[2] D. I. Khomskii and T. Mizokawa, Phys. Rev. Lett. **94**, 156402 (2005).
[3] D. I. Khomskii and S. V. Streltsov, Chem. Rev. **121**, 2992 (2021).
[4] M. Isobe and Y. Ueda, J. Phys. Soc. Jpn. **71**, 1848 (2002).
[5] M. Schmidt, W. Ratcliff, P. G. Radaelli, K. Refson, N. M. Harrison, and S. W. Cheong, Phys. Rev. Lett. **92**, 056402 (2004).
[6] H. D. Zhou and J. B. Goodenough, Phys. Rev. B **72**, 045118 (2005).
[7] F. J. Morin, Phys. Rev. Lett. **3**, 34 (1959).
[8] L. L. Van Zandt, J. M. Honig, and J. B. Goodenough, J. Appl. Phys. **39**, 594 (1968).
[9] W. R. Robinson, J. Solid State Chem. **9**, 255 (1974).
[10] C. E. Rice and W. R. Robinson, Acta Cryst. B **33**, 1342 (1977).
[11] H. J. Zeiger, Phys. Rev. B **11**, 5132 (1975).
[12] L. F. Mattheiss, J. Phys.: Condens. Matter **8**, 5987 (1996).
[13] A. Tanaka, J. Phys. Soc. Jpn. **73**, 152 (2004).
[14] A. I. Poteryaev, A. I. Lichtenstein, and G. Kotliar, Phys. Rev. Lett. **93**, 086401 (2004).
[15] V. Eyert, U. Schwingenschlögl, and U. Eckern, Europhys. Lett. **70**, 782 (2005).
[16] H. Sato, A. Tanaka, M. Sawada, F. Iga, K. Tsuji, M. Tsubota, M. Takemura, K. Yaji, M. Nagira, A. Kimura, T. Takabatake, H. Namatame, and M. Taniguchi, J. Phys. Soc. Jpn. **75**, 053702 (2006).
[17] C. F. Chang, T. C. Koethe, Z. Hu, J. Weinen, S. Agrestini, L. Zhao, J. Gegner, H. Ott, G. Panaccione, Hua Wu, M. W. Haverkort, H. Roth, A. C. Komarek, F. Offi, G. Monaco, Y.-F. Liao, K.-D. Tsuei, H.-J. Lin, C. T. Chen, A. Tanaka *et al.*, Phys. Rev. X **8**, 021004 (2018).
[18] S. Torigoe, T. Hattori, K. Kodama, T. Honda, H. Sagayama, K. Ikeda, T. Otomo, H. Nitani, H. Abe, H. Murakawa, H. Sakai, and N. Hanasaki, Phys. Rev. B **98**, 134443 (2018).
[19] T. Yamaguchi, M. Okawa, H. Wadati, T. Z. Regier, T. Saitoh, Y. Takagi, A. Yasui, M. Isobe, Y. Ueda, and T. Mizokawa, J. Phys. Soc. Jpn. **91**, 074704 (2022).

[20] K. Yoshimatsu, H. Mashiko, N. Umezawa, K. Horiba, H. Kumigashira, and A. Ohtomo, J. Phys. Chem. C **121**, 18717 (2017).
[21] U. O. Bhagwat, J. J. Wu, A. M. Asiri, and S. Anandan, ChemistrySelect **4**, 788 (2019).
[22] D. Morris, Y. Dou, J. Rebane, C. E. J. Mitchell, R. G. Egdell, D. S. L. Law, A. Vittadini, and M. Casarin, Phys. Rev. B **61**, 13445 (2000).
[23] S. Dash, T. Kajita, M. Okawa, T. Saitoh, E. Ikenaga, N. L. Saini, T. Katsufuji, and T. Mizokawa, Phys. Rev. B **97**, 165116 (2018);
[24] S. Dash, T. Kajita, M. Okawa, T. Saitoh, E. Ikenaga, N. L. Saini, T. Katsufuji, and T. Mizokawa, Phys. Rev. B **99**, 079901(E) (2019).
[25] K. Momma and F. Izumi, J. Appl. Cryst. **44**, 1272 (2011).
[26] K. Takasu, M. Arizono, T. Shirasaki, H. Kuwahara, T. Yoshida, T. Katsufuji, and T. Okuda, *Proceedings of the 29th International Conference on Low Temperature Physics (LT29), Sapporo, Japan* (2022).
[27] J. Weinen, T. C. Koethe, C. F. Chang, S. Agrestini, D. Kasinathan, Y. F. Liao, H. Fujiwara, C. Schler-Langeheine, F. Strigari, T. Haupricht, G. Panaccione, F. Offi, G. Monaco, S. Huotari, K.-D. Tsuei, and L. H. Tjeng, J. Electron Spectrosc. Relat. Phenom. **198**, 6 (2015).
[28] J. J. Yeh and I. Lindau, At. Data Nucl. Data Tables **32**, 1 (1985).
[29] M. B. Trzhaskovskaya, V. I. Nefedov, and V. G. Yarzhemsky, At. Data Nucl. Data Tables **77**, 97 (2001).
[30] M. B. Trzhaskovskaya, V. I. Nefedov, and V. G. Yarzhemsky, At. Data Nucl. Data Tables **82**, 257 (2002).
[31] D. Takegami, L. Nicolaï, T. C. Koethe, D. Kasinathan, C. Y. Kuo, Y. F. Liao, K. D. Tsuei, G. Panaccione, F. Offi, G. Monaco, N. B. Brookes, J. Minár, and L. H. Tjeng, Phys. Rev. B **99**, 165101 (2019).
[32] T. Yasuda, Y. Kondo, T. Kajita, K. Murota, D. Ootsuki, Y. Takagi, A. Yasui, N. L. Saini, T. Katsufuji, and T. Mizokawa, Phys. Rev. B **102**, 205133 (2020).
[33] S. A. Chambers, M. H. Engelhard, L. Wang, T. C. Droubay, M. E. Bowden, M. J. Wahila, N. F. Quackenbush, L. F. J. Piper, T.-L. Lee, C. J. Nelin, and P. S. Bagus, Phys. Rev. B **96**, 205143 (2017).
[34] N. Hasegawa, K. Yoshimatsu, D. Shiga, T. Kanda, S. Miyazaki, M. Kitamura, K. Horiba, and H. Kumigashira, Phys. Rev. B **105**, 235137 (2022).
[35] R. Takahama, T. Ishii, D. Indo, M. Arizono, C. Terakura, Y. Tokura, N. Takeshita, M. Noda, H. Kuwahara, T. Saiki, T. Katsufuji, R. Kajimoto, and T. Okuda, Phys. Rev. Mater. **4**, 074401 (2020).
[36] D. Takegami, L. Nicolaï, Y. Utsumi, A. Meléndez-Sans, D. A. Balatsky, C.-A. Knight, C. Dalton, S.-L. Huang, C.-S. Chen, L. Zhao, A. C. Komarek, Y.-F. Liao, K.-D. Tsuei, J. Minár, and L. H. Tjeng, Phys. Rev. Res. **4**, 033108 (2022).